Biochemical and Biophysical Research Communications 381 (2009) 12–15

Contents lists available at ScienceDirect

Biochemical and Biophysical Research Communications

journal homepage: www.elsevier.com/locate/ybbrc

Kinetic and structural studies of the role of the active site residue Asp235 of human pyridoxal kinase

Amit K. Gandhi [a], Mohini S. Ghatge [a], Faik N. Musayev [a], Aaron Sease [b], Samuel O. Aboagye [c], Martino L. di Salvo [d], Verne Schirch [a], Martin K. Safo [a,*]

[a] Department of Medicinal Chemistry, School of Pharmacy and Institute for Structural Biology and Drug Discovery, Virginia Commonwealth University, 800 East Leigh Street, Suite 212, Richmond VA 23219, USA
[b] Department of Natural Sciences, Virginia Union University, Richmond, VA 23220, USA
[c] Department of Chemistry, Virginia Commonwealth University, Richmond VA 23284, USA
[d] Istituto Pasteur—Fondazione Cenci Bolognetti, Dipartimento di Scienze Biochimiche, Università La Sapienza Roma, Italy

ARTICLE INFO

Article history:
Received 21 January 2009
Available online 4 February 2009

Keywords:
Pyridoxal kinase
Ribokinase
Pyridoxal 5′-phosphate
Crystallography
Vitamin B_6
Substrate inhibition
Catalysis
Phosphorylation

ABSTRACT

Pyridoxal kinase catalyzes the phosphorylation of pyridoxal (PL) to pyridoxal 5′-phosphate (PLP). A D235A variant shows 7-fold and 15-fold decreases in substrate affinity and activity, respectively. A D235N variant shows ~2-fold decrease in both PL affinity and activity. The crystal structure of D235A (2.5 Å) shows bound ATP, PL and PLP, while D235N (2.3 Å) shows bound ATP and sulfate. These results document the role of Asp235 in PL kinase activity. The observation that the active site of PL kinase can accommodate both ATP and PLP suggests that formation of a ternary Enz·PLP·ATP complex could occur in the wild-type enzyme, consistent with severe MgATP substrate inhibition of PL kinase in the presence of PLP.

Pyridoxal 5′-phospate (PLP) is the active form of vitamin B_6 used by several apo-B_6 enzymes as a co-factor to form the catalytically competent holo-enzymes serving vital roles in various transamination, decarboxylation, and synthesis pathways involving carbohydrates, sphingolipids, amino acids, heme and neurotransmitters [1–2]. Mammals cannot synthesize PLP from small metabolites by a *de novo* pathway but require the dietary B_6 vitamins; pyridoxal (PL) or pyridoxine or pyridoxamine via a salvage pathway. In the presence of MgATP, PL kinase catalyzes the addition of phosphate to the 5′ alcohol of pyridoxine, pyridoxamine and PL to form pyridoxine 5′-phosphate, pyridoxamine 5′-phosphate and PLP, respectively, [3]. Pyridoxine 5′-phosphate and pyridoxamine 5′-phosphate are subsequently converted to PLP by pyridoxine 5′-phosphate oxidase [3].

Disruption of the salvage pathway, due to mutation or inhibition of PL kinase or lack of vitamin B_6 intake is known to result in PLP deficiency, which is implicated in several pathologies, most notably neurological disorders since syntheses of many neurotransmitters involve PLP-dependent enzymes [4–10]. An emerging health problem is the intake of too much vitamin B_6. In various studies, high doses of the highly reactive PLP in the cell also exhibits toxic effects, including sensory and motor neuropathies due to its propensity to react with several nucleophiles [11].

The reaction mechanism of PL kinases involves random sequential substrate addition, with the metal ion tandem Mg^{2+} and K^+ required for enzyme activity [12–14]. The crystal structures of *Escherichia coli*, sheep and human PL kinases reveal a functional dimeric structure, with one active site per each monomer [12–14]. PL kinases are classified as members of the ribokinase superfamily, since they show the same typical central core tertiary structures of β-sheets surrounded by α-helices, as well as conserved ATP and substrate binding site geometries [12–15]. Members of this enzyme superfamily catalyze the phosphorylation of the C5′-hydroxyl group of their respective substrates using ATP. In PL kinases and in the ribokinase superfamily as a whole, a conserved Asp235 residue is observed to make a hydrogen-bond interaction with the C5′—OH group of the substrates, and the current working hypothesis suggests this residue to be the base that deprotonates the C5′—OH group, with the resulting negatively charged O5′ atom making a direct nucleophilic attack on the ATP γ-phosphate (Scheme 1) [12–15]. Our goal is to determine if Asp235 plays a catalytic role in PL kinase enzymatic activity.

* Corresponding author. Fax: +1 804 827 3664.
E-mail address: msafo@vcu.edu (M.K. Safo).

0006-291X/$ - see front matter © 2009 Elsevier Inc. All rights reserved.
doi:10.1016/j.bbrc.2009.01.170

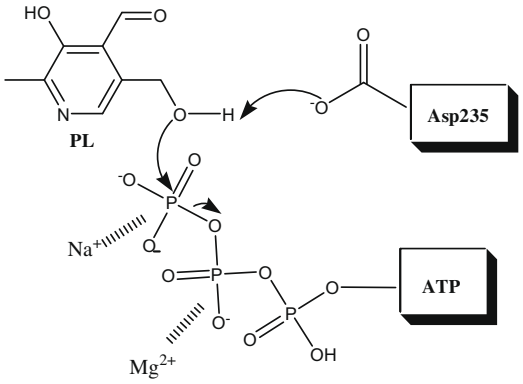

Scheme 1. Proposed reaction mechanism by PL kinase.

Materials and methods

Site-directed mutagenesis and enzyme production. The variants were made on the wild-type construct pET22b(+) carrying the human *pdx*K gene insert [16] using the QuickChange™ Site-Directed Mutagenesis Kit from Stratagene (La Jolla, CA). The mutations were confirmed by sequencing the cDNA inserts. The *pdx*K gene inserts were then transferred into a pET28a(+) vector by use of NdeI and XhoI unique restriction sites. The new constructs were then transformed into *E. coli* Rosetta (λDE3) pLysS competent cells for protein expression (Novagen, EMD Chemicals Inc., Merck KGaA, Darmstadt, Germany).

The Rosetta cells with the mutated genes were grown in 6L of LB-kanamycin–chloramphenicol medium to an optimal density of 1.2 at 600 nm, and then induced with 0.5 mM IPTG. Cells were grown for an additional 5 h at 32 °C and harvested by centrifugation. The cell pellets were resuspended in 250 ml of 50 mM sodium phosphate buffer, pH 8.0, and disrupted by osmotic shock. Streptomycin sulfate was added to a final concentration of 10 g/L to remove excess nucleic acids. The enzyme was dialyzed in 50 mM sodium phosphate buffer, pH 8.0, and then purified using a Ni-NTA column [14]. Fractions containing 95% purity, as judged by SDS-Page were pooled and concentrated.

Determination of kinetic constants. Wild-type, and D235A and D235N variant forms used in the kinetic experiments were dialyzed overnight against 20 mM sodium BES buffer, pH 7.2. Kinetic assays were performed at 37 °C in 1 cm thermostated cuvette. Initial velocity studies for the conversion of PL to PLP were followed at 388 nm in an Agilant 8454 spectrophotometer in 20 mM sodium BES buffer, pH 7.2, [14,16]. MgATP concentrations were varied between 100 to 800 μM, and PL concentrations between 20 to 300 μM. The K_m and k_{cat} values for PL and MgATP were determined by double reciprocal plots constructed with Sigma Plot and the results shown in Table 1.

Crystallization and data collection. Crystallization drops were composed of 2.5 mL of protein solution (with 2.5 mM MgATP and/or 1 mM PL) and 2.5 mL of reservoir and equilibrated against 700 mL reservoir solution (100 mM Tris–HCl, pH 8.0, and 57% MPD, 5 mM $MgSO_4$). Crystals were cryoprotected in solution containing 100 mM Tris–HCl buffer (pH 8.0) and 60% MPD with the appropriate substrates before flash cooling. X-ray data were collected at 100 K using a Molecular Structure Corporation (MSC) X-Stream Cryogenic Crystal Cooler System and an R-Axis IV++ image plate detector, a Rigaku MicroMax–007 X-ray source equipped with MSC Varimax confocal optics operating at 40 kV and 20 mA. The data were processed with the MSC d*trek software and the CCP4 suite of programs [17]. The X-ray data from the D235N and D235A are summarized in Table 2.

Structure refinement. The isomorphous human PL kinase structure (PDB code 2YXU), mutating Asp235 to Gly, and omitting bound ATP, phosphate, water and MPD molecules was used as the starting model for the refinements of the two variant structures. All refinements were performed with the CNS program [18]. After rigid body refinement, conjugate gradient minimization and simulated annealing using the diffraction data of D235A, difference density at residue 235 suggested an Ala consistent with nucleotide sequencing result. Densities were also identified for ATP, Mg^{2+} and Na^{+} in both active sites. We also observed bound PLP and PL molecules in the active site of subunit B (Fig. 1A and B), and bound PL and sulfate molecules in the active site of subunit A.

In the D235N variant, after a similar refinement cycle, using a model with residue 235 as Gly, we observed a density extending from the α-carbon of residue 235 suggesting an Asn mutation (Fig. 1C and D). We also observed in the active sites, bound ATP and sulfate molecules. The two complexes were refined with alternate cycles of conjugate gradient minimization, simulated annealing and B-factor refinements with intermittent model rebuilding using both TOM [19] and COOT [20]. Addition of water, MPD and sulfate molecules led to the final crystallographic *R*free/*R*-factors of 21.2%/26.2% for the 2.5 Å resolution D235A structure; and 21.4%/26.1% for the 2.3 Å resolution D235N structure. The structure solution/refinement statistics are shown in Table 2. All figures were drawn using PyMOL (Delano Scientific, 2007; http://www.pymol.org) and labels were added using Adobe® Photoshop. Atomic coordinates and structure factors have been deposited in the RCSB Protein Data Bank with codes 3FHX and 3FHY for D235A and D235N, respectively.

Table 1
Kinetic parameters for human PL kinase.

Enzyme	Wild-type	D235N	D235A
K_m, PL (μM)	24	58	170
K_m, MgATP (μM)	190	180	170
k_{cat} (min^{-1})	29	14	1.9

Table 2
Crystal information, data collection and refinement parameters.[a]

	D235A	D235N
Data collection statistics		
Space group	I222	I222
Cell dimensions (Å)	91.2 115.4 168.9	91.1 114.6 169.7
Resolution (Å)	32.69–2.5 (2.59–2.5)	32.54–2.30 (2.38–2.30)
No. of measurements	124056	133496
Unique reflections	31128 (2935)	39415(3745)
I/sigma I	10.9 (4.2)	15.5 (4.6)
Completeness (%)	99.7 (99.6)	99.0 (99.3)
Redundancy	3.99 (3.79)	3.39 (3.18)
Rmerge (%)[b]	8.3 (29.8)	4.9 (25.0)
Structure refinement		
Resolution limit (Å)	29.93–2.5 (2.59–2.5)	29.36–2.30 (2.38–2.30)
No. of reflections	31124 (2935)	39410 (3745)
R-factor (%)	21.2 (38.9)	21.4 (38.2)
Rfree (%)[c]	26.2 (40.3)	26.1(43.8)
Rmsd standard geometry		
Bond-lengths (Å)/-angles (°)	0.008/1.4	0.008/1.4
Most favored/allowed regions	93.6/5.7	93.9/5.3
B-factors		
All atoms/protein atoms	43.8/43.2	44.2/43.4
ATP/metal ions	40.7/35.3	38.5/28.4
Sulfate/water/MPD	72.3/40.1/75.7	74.1/45.8/72.2

[a] Numbers in parenthesis refer to the outermost resolution bin.
[b] Rmerge = $\Sigma_{hkl}\Sigma_i \mid I_{hkli} - \langle I_{hkli}\rangle \mid \Sigma_{hkl}\Sigma_i\langle I_{hkli}\rangle$.
[c] Rfree calculated with 5% of excluded reflection from the refinement.

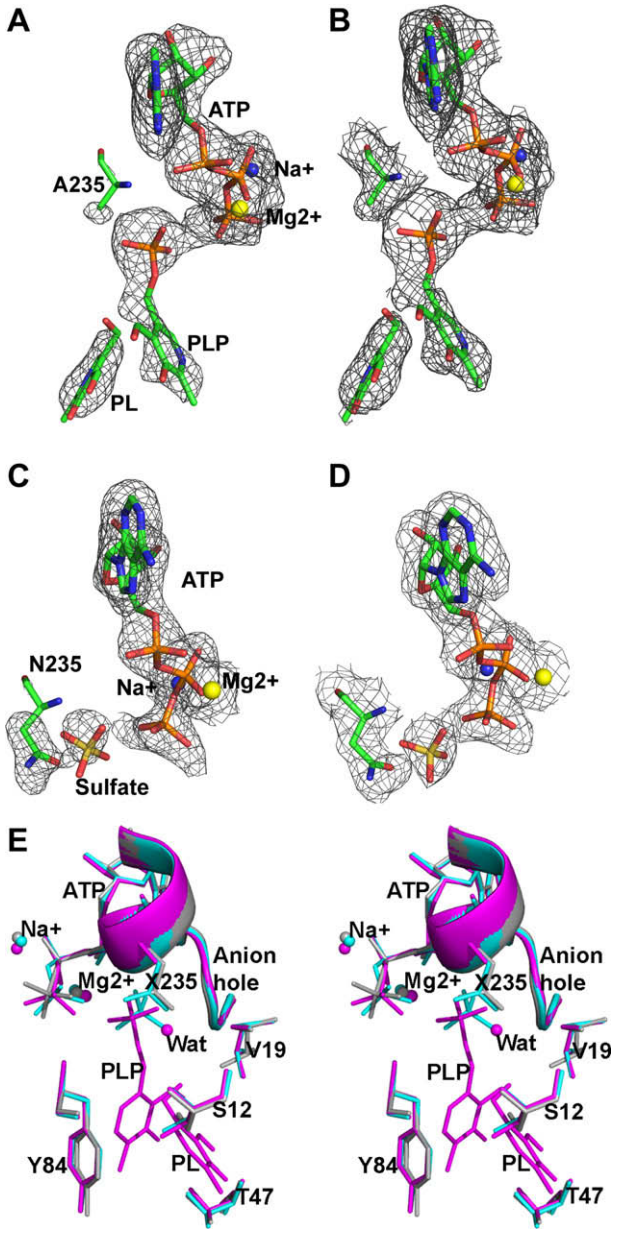

Fig. 1. Crystal Structure of PL kinase. (A) A Fo–Fc map (contoured at 2.6σ level) of the D235A model calculated before Na^+, Mg^{2+}, PLP, PL, ATP and Ala235 side-chain were added to the subunit B active site. (B) A 2Fo–Fc map (0.8σ level) of the subunit B active site of the D235A model. (C) A Fo–Fc map (2.6σ level) of the D235N model calculated before Na^+, Mg^{2+}, sulfate, and Asn235 side-chain were added to the subunit B active site. (D) A 2Fo–Fc map (0.8σ level) of the subunit B active site of the D235N model. All maps are superimposed with the final refined models. (E) Stereo view comparison of the active site of the wild-type structure in complex with ATP (grey), D235N in complex with ATP and sulfate (cyan), and D235A in complex with PLP, PL, ATP and the non-conserved water (magenta). Residue 235 is labeled as X235. Also shown are the cation positions. (For interpretation of the references to color in this figure legend, the reader is referred to the web version of this paper.)

Results and discussion

The variants D235A and D235N were constructed, expressed and purified. The D235A variant showed a 15-fold decrease in catalytic activity, as well as a 7-fold decrease in affinity for PL (Table 1). The D235N mutation resulted in a ~2-fold decrease in activity and PL affinity. The K_m for MgATP did not change significantly between the wild-type and variant enzymes, consistent with the fact that the carboxylate of Asp235 makes a hydrogen-bond interaction with PL but not with ATP.

The D235A and D235N variant structures were refined to 2.5 and 2.3 Å, respectively, using the isomorphous wild-type structure (PDB code 2YXU). The D235A variant structure, co-crystallized with PL and ATP, showed these two substrates, as well as the product PLP bound simultaneously at the subunit B active site (Fig. 1A and B). In subunit A, we also observed PL and ATP, but instead of PLP, we found a bound sulfate molecule that occupies the PLP phosphate position. The D235N variant, co-crystallized with only ATP, shows bound ATP and the sulfate molecule described above (Fig. 1C and D). The sulfate molecules could be coming from $MgSO_4$ used in the crystallization experiment. However, we cannot rule out the possibility that this anion is phosphate that results from spontaneous hydrolysis of ATP γ-phosphate, which is known to happen in PL kinase [12]. The PLP phosphate moiety or the sulfate molecule lies adjacent to the ATP γ-phosphate, and are stabilized by a P-loop, consisting of an anion hole formed by the highly conserved sequence motif GTGA (residues 231–234) and the N-terminus of the helix formed by the residues 234–248. The PLP phosphate or the sulfate molecule makes extensive hydrogen-bond interactions with the backbone nitrogen atoms of the anion hole residues, while the rest of the PLP molecule is located inside the active site with very limited protein contacts, consistent with a weaker PLP ring density. The ATP γ-phosphate is further stabilized by a bound Na^+, while the β-phosphate is stabilized by the P-loop and Mg^{2+}.

Comparisons of the D235A, D235N and the wild-type structures show similar folds with root mean square deviations of ~0.2 Å. The ATP and PL binding site geometries, as well as their associated interactions with the protein are also conserved (Fig. 1E). In the D235N variant, the side-chain of Asn235 occupies the same position as the wild-type Asp235 side chain and makes a conserved hydrogen-bond interaction with the C5′-OH group of a modeled PL. In the D235A variant, there is a non-conserved water molecule close to the Asp235 carboxylate oxygen atom (Fig. 1E). The water is close to the amide nitrogen of Gly20 (~3 Å), as well as the C5′—OH group of PL (~3 Å). The bound PL makes conserved PL kinase interactions with the residues Ser12, Thr47, Val19 and Tyr84.

This study suggests that Asp235 is the catalytic base involved in PL kinase activity. The study, however, unexpectedly showed less than the anticipated drop in variant catalytic activities, which would be consistent with removal of an essential catalytic base. Since the human PL kinase enzyme was purified with a His-tag affinity column, significant contamination by wild-type enzyme is ruled out. Most likely, the ~7% activity of the D235A variant could be attributed to the non-conserved water molecule described above acting as a weak base. As noted above the ATP γ-phosphate is known to hydrolyze spontaneously, which suggests that even a weak catalytic base could initiate the phosphorylation reaction, consistent with the significant activity of the D235N mutant. We propose that during the catalytic reaction, Asp235 forms a strong H-bond with the 5′—OH of PL to enhance the nucleophilicity of the substrate. A subsequent nucleophilic attack by PL on the ATP γ-phosphate results in the transfer of the proton from the 5′—OH group to the Asp235 carboxyl group, and concomitant transfer of the γ-phosphate to PL.

The reduced rate of PL phosphorylation by the D235A variant might have led to the trapping of ATP, PL and PLP at the active site. The ability to trap a PLP in the presence of the MgATP substrate suggests that PL kinase might use this mechanism to self-regulate its activity. This is consistent with our previously published kinetic study with *E. coli* PL kinase that showed severe MgATP inhibition of the enzyme in the presence of PLP. [13] We speculate that this inhibition is due to formation of a non-productive PL kinase·PLP·ATP complex.

Acknowledgment

The structural biology resources used in this study provided in-part by the National Cancer Institute of the National Institutes of Health to the VCU Massey Cancer Center [Grant CA 16059-28].

References

[1] D.B. McCormick, Biochemistry of coenzymes, in: R.A. Meyers (Ed.), Encyclopedia of Molecular Biology and Molecular Medicine, vol. 1, VCH, Weinheim, Germany, 1996, pp. 396–406.
[2] J.E. Leklem, Vitamin B-6, in: L. Machlin (Ed.), Handbook of Vitamins, Marcel Decker Inc., New York, 1991, pp. 341–378.
[3] D.B. McCormick, H. Chen, Update on interconversions of vitamin B-6 with its coenzyme, J. Nutr. 129 (1999) 325–327.
[4] H.B. Mills, A.H. Robert, M.P. Surtees, C.E. Champion, N.D. Beesley, J.S. Peter, J.R. Simon, A.B. Heales, S. Irene, G.F. Hoffmann, J. Zschocke, T.C. Peter, Neonatal epileptic encephalopathy caused by mutations in the PNPO gene encoding pyridox(am)ine 5-phosphate oxidase, Hum. Mol. Genet. 14 (2005) 1077–1086.
[5] S. Song, S. Ueno, J.I. Numata, S. Shibuya-Tayoshi, M. Nakataki, S. Tayoshi, K. Yamauchi, S. Sumitani, T. Tomotake, T. Tada, T. Tanahashi, M. Itakura, T. Ohmori, Association between PNPO and schizophrenia in the Japanese population, Schizophr. Res. 97 (2007) 264–270.
[6] P. Laine-Cessac, A. Cailleux, P. Allain, Mechanisms of the inhibition of human erythrocyte pyridoxal kinase by drugs, Biochem. Pharmacol. 54 (1997) 863–870.
[7] D.W. Jacobsen, Homocysteine and vitamins in cardiovascular disease, Clin. Chem. 8 (1998) 1833–1843.
[8] S.N. Meydani, J.D. Ribaya-Mercado, R.M. Russell, N. Sahyoun, F.D. Morrow, S. Gershoff, Vitamin B-6 deficiency impairs interleukin 2 production and lymphocyte proliferation in elderly adults, Am. J. Clin. Nutr. 53 (1991) 1275–1280.
[9] J.B. Adams, F. George, T. Audhya, Abnormally high plasma levels of vitamin B6 in children with autism not taking supplements compared to controls not taking supplements, J. Altern. Complement. Med. 12 (2006) 59–63.
[10] S.P. Coburn, J.D. Mahuren, W.E. Schaltenbrand, Increased activity of pyridoxal kinase in tongue in Down's syndrome, J. Ment. Defic. Res. 35 (1991) 543–547.
[11] L. Philippe, P. Andrea, G. Mireille, Pyridoxine in clinical toxicology: a review, Euro. J. Emergency. Med. 12 (2005) 78–85.
[12] M.H. Li, F. Kwok, W.R. Chang, C.K. Lau, J.P. Zhang, S.O. Liu, Y.C. Leung, T. Jiang, D.C. Liang, Crystal structure of brain pyridoxal kinase, a novel member of the ribokinase superfamily, J. Biol. Chem. 277 (2002) 46385–46390.
[13] M.K. Safo, F.N. Musayev, S. Hunt, M.L. Di Salvo, J.-B. Claude, V. Schirch, Crystal structure of pyridoxal kinase from the *Escherichia coli* pdxK gene: implications for the classification of pyridoxal kinases, J. Bacteriol. 188 (2006) 4542–4552.
[14] F.N. Musayev, M.L. Di Salvo, T.-P. Ko, A.K. Gandhi, A. Goswami, V. Schirch, M.K. Safo, Crystal Structure of human pyridoxal kinase: structural basis of M^{+} and M^{2+} activation, Protein Sci. 16 (2007) 2184–2194.
[15] I.I. Mathews, M.D. Erion, S.E. Ealick, Structure of human adenosine kinase at 1.5 Å resolution, Biochemistry 37 (1998) 15607–15620.
[16] M.L. Di Salvo, S. Hunt, V. Schirch, Expression, purification and kinetic constants for human and *Escherichia coli* pyridoxal kinases, Protein Expr. Purif. 36 (2004) 300–306.
[17] The CCP4 suite: programs for protein crystallography, Acta Crystallogr. D50 (1994) 760–763.
[18] A.T. Brunger, P.D. Adams, G.M. Clore, W.L. DeLano, P. Gros, R.W. Grosse-Kunstleve, J.S. Jiang, J. Kuszewski, M. Nilges, N.S. Pannu, R.J. Read, L.M. Rice, T. Simonson, G.L. Warren, Crystallography and NMR system: a new software suite for macromolecular structure determination, Acta Crystallogr. D 54 (1998) 905–921.
[19] C. Cambillau, E. Horjales, TOM: a frodo subpackage for protein-ligand fitting with interactive energy minimization, J. Mol. Graph. 5 (1987) 74–177.
[20] P. Emsley, K. Cowtan, COOT: model-building tools for molecular graphics, Acta Cryst. D 60 (2004) 2126–2132.